Applied Surface Science 259 (2012) 791–798

Contents lists available at SciVerse ScienceDirect

Applied Surface Science

journal homepage: www.elsevier.com/locate/apsusc

Influence of the surface morphology on the early stages of Cu oxidation

Langli Luo[a], Yihong Kang[b], Judith C. Yang[c], Guangwen Zhou[a,*]

[a] Department of Mechanical Engineering & Multidisciplinary Program in Materials Science and Engineering, State University of New York, Binghamton, NY 13902, United States
[b] Department of Mechanical Engineering and Materials Science, University of Pittsburgh, Pittsburgh, PA 15261, United States
[c] Department of Chemical and Petroleum Engineering, University of Pittsburgh, Pittsburgh, PA 15261, United States

ARTICLE INFO

Article history:
Received 29 April 2012
Received in revised form 10 July 2012
Accepted 20 July 2012
Available online 27 July 2012

Keywords:
Surface morphology
Oxidation
Copper
Electron microscopy
Atomic force microscopy

ABSTRACT

The growth and morphological features of Cu films deposited on NaCl(1 0 0) by e-beam evaporation have been examined to evaluate the effect of various surface morphologies on the initial oxidation of Cu. It is shown that epitaxial Cu films with significantly reduced surface roughness can be achieved by first nucleating Cu seeds at 450 °C that favors epitaxial Cu grains which is followed by subsequent seed growth at 150 °C that favors smooth Cu film. The effect of the variations of the surface morphology of the resulting Cu films by the different growth conditions on the early stages oxidation of Cu films is examined by *in situ* transmission electron microscopy (TEM) and *ex situ* atomic force microscopy (AFM). It is shown that the changes in the surface morphologies of the Cu film result in distinct variations in the nucleation density and growth rates of oxide islands. Such correlation between the surface morphology and the initial oxidation behavior of the Cu films provides insights into understanding the microscopic processes of the transient oxidation of metals and for manipulating the initial oxide formation through surface treatments.

© 2012 Elsevier B.V. All rights reserved.

1. Introduction

The morphology and crystallographic structure of surfaces and interfaces is of great importance in basic surface science as well as many technological applications, *e.g.*, thin film processing [1,2], electrical properties of thin insulating film capacitor [3,4], device performance of organic light emitting device [5]. Specifically, surface roughness plays a significant role in the field of metal oxidation, *e.g.*, the integrity of thermally generated oxide scale on metal surface [6] used as thermal barrier coating and the change of oxide patterns formed on Au surface [7] for heterogeneous catalysis. Traditionally, much attention has been paid to the morphology and growth kinetics of oxide film or scale on metal surface. The early stages of metal oxidation involving nucleation and growth of oxide islands become more vital in the nanoscale oxidation. For instance, the environmental stability of Cu metallization widely used in ultra-large scale integration circuits becomes a critical issue when the dimensions of fabricated semiconductor devices shrink to the nanoscale [8–10]. The morphological evolution and microstructural development of Cu films during deposition are strongly related to the processing and the reliability of interconnection metallization films [11]. Grainy structure, as measured by the grain size and grain size distribution, and crystallographic texture are important attributes, which determine the performance of Cu interconnections [12]. Cu films deposited on amorphous substrates exhibit specific and random textures [13] while epitaxial Cu films can be deposited on single crystal substrates [14,15].

The oxidation of metals involves hierarchical multiple length scales and proceeds from oxygen chemisorption and surface reconstruction to oxide nucleation and growth and then to the formation of a continuous, macroscopically thick oxide layer. Perfect surfaces are usually preferred for the study of the initial-stage oxidation of oxygen adsorption and surface reconstructions involving ultra-high vacuum (UHV) techniques. However, real surfaces are far from perfect containing a large number of defects such as surface steps, vacancies and grain boundaries. Our understanding of the effect of these surface defects on the early stages oxidation of metals is still very limited. *In situ* environmental transmission electron microscopy (TEM) is one of the few tools with the sufficient spatial resolution for studying the role of surface defects on the nucleation and growth of oxide islands during the early stages of oxidation of metals. By introducing reactive gas to specimens under elevated temperature, *in situ* TEM experiments provide dynamic information from nucleation to growth and coalescence of oxide islands at nanometer scale under the controlled oxidation conditions, which is inaccessible by both surface science and traditional bulk oxidation study methods, but is essential for understanding the atomistic initial-stage oxidation kinetics.

It has been shown that crystallographic defects such as dislocations and stacking faults in Cu films have a minor effect on the oxide nucleation and growth [16], but significant surface roughness can enhance the nucleation of oxide islands [17]. In this present work,

* Corresponding author. Tel.: +1 607 777 5084; fax: +1 607 777 4620.
E-mail address: gzhou@binghamton.edu (G. Zhou).

0169-4332/$ – see front matter © 2012 Elsevier B.V. All rights reserved.
http://dx.doi.org/10.1016/j.apsusc.2012.07.125

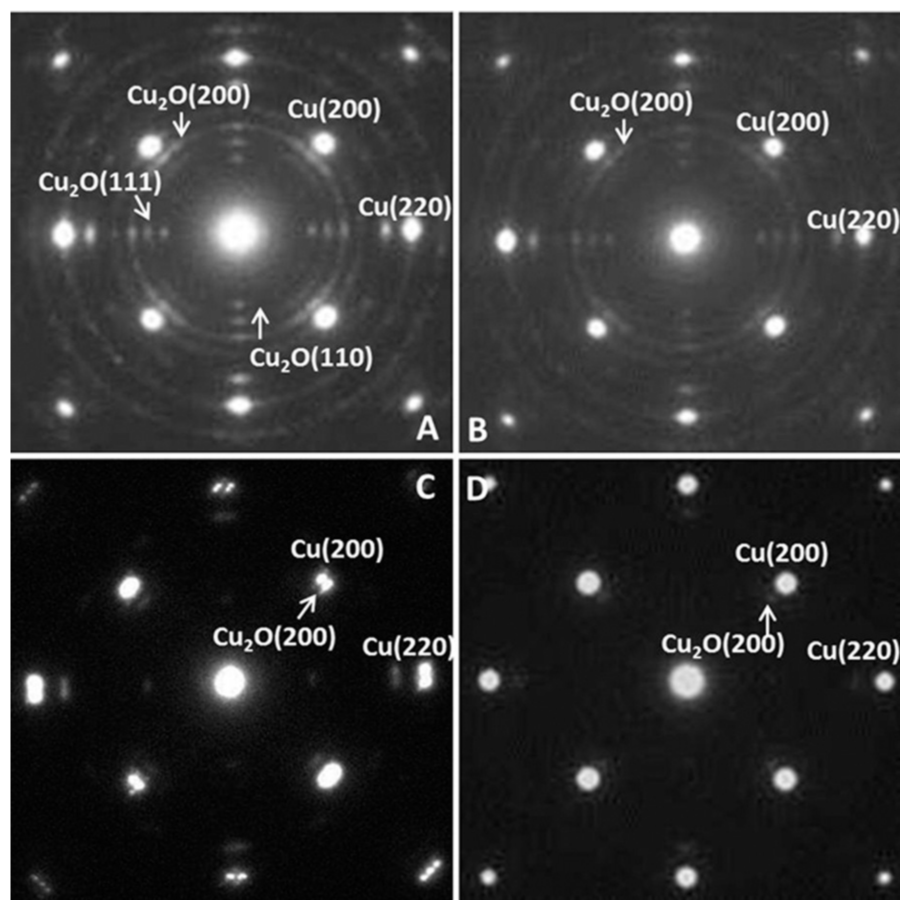

Fig. 1. SAED patterns of Cu thin films deposited on NaCl(1 0 0) substrates at (A) 150 °C, (B) 250 °C, (C) 350 °C and (D) 450 °C.

we tackle this problem by examining the initial oxidation of Cu films deposited on NaCl(1 0 0) substrates, where the Cu thin films with different morphologies and grain structures are prepared by changing the thin film deposition conditions. Our results demonstrate that the nucleation and growth of oxide islands during the oxidation of the Cu films can be significantly influenced by the surface morphologies of the Cu films.

2. Experimental

Single crystal Cu(1 0 0) thin films were deposited on NaCl(1 0 0) substrates in an ultra-high vacuum (UHV) electron-beam evaporator with a deposition rate of 1 Å/s. The NaCl(1 0 0) substrates were freshly cleaved from NaCl crystal cubes. The thickness of 700 Å of Cu films was chosen so that the metal films were electron transparent to be examined by the TEM and also retain the oxidation behavior as close as to that of bulk metal. The Cu thin films were removed from NaCl substrates by floating in deionized water, washed and mounted on a specially designed TEM holder that allows for resistive heating up to ~1000 °C. Our *in situ* oxidation experiments were carried out in a modified JEOL 200CX TEM. This microscope is equipped with an UHV chamber with a base pressure at $\sim 10^{-8}$ Torr. A leak valve attached to the column permits introduction of gases directly into the TEM column with a controlled oxygen gas pressure (pO_2) ranging from 5×10^{-5} Torr to 760 Torr, which can be monitored by a full range vacuum gauge. Before the oxidation experiments, any native oxide was removed by annealing the Cu films in the TEM column at 750 °C under vacuum condition [18,19] or *in situ* annealing under H_2 gas at the pressure $\sim 10^{-5}$ Torr and 350 °C, resulting in a clean metal surface. The sample cleanliness was checked by X-ray energy dispersive spectroscopy (EDS) analysis and electron diffraction. Oxygen gas of 99.999% purity was then admitted into the column of the microscope through the leak valve to oxidize clean Cu films. The structural and morphological evolution of oxide nucleation and growth were monitored *in situ* by TEM imaging and electron diffraction under the controlled oxidation temperature and oxygen pressure. As-deposited and post-oxidized Cu surfaces were also examined by atomic force microscopy (AFM).

3. Results and discussion

3.1. Epitaxy of Cu films

Cu(1 0 0) films are deposited on NaCl(0 0 1) substrates at temperature ranging from 150 °C to 450 °C to study the growth morphology and crystallographic relation between the films and substrates. TEM imaging and selected area electron diffraction (SAED) is employed to examine the dependence of film morphology and epitaxial relation on the film deposition temperature. As shown in Fig. 1, the SAED patterns of as-deposited Cu thin films reveal that Cu(0 0 1) films can be epitaxially grown on NaCl(1 0 0) substrate at temperatures ranging from 150 °C to 450 °C. The strong spots resulting from Cu diffracted beams show a face-centered cubic (FCC) pattern with the zone axis of [0 0 1] direction, indicating that the epitaxial relationship, *e.g.*, (0 0 1)Cu//(0 0 1)NaCl and [0 0 1]Cu//[0 0 1]NaCl is maintained for the deposition temperature above 150 °C. However, the diffraction patterns (*e.g.*, Fig. 1(A) and (B)) from Cu films deposited at the temperatures of 150 °C and 250 °C show diffraction rings superimposed on the Cu(2 0 0) and (2 2 0) spots, suggesting the growth of randomly oriented Cu grains

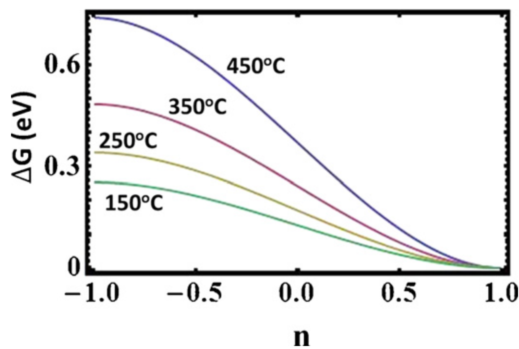

Fig. 2. Plots of the nucleation barrier ΔG^* *vs.* the interaction parameter n at different substrate temperatures for Cu deposition on NaCl substrate.

in addition to epitaxial Cu grains. With increase in the deposition temperature, the intensity of the diffraction rings decreases and the diffraction ring pattern completely disappear in the Cu film deposited at 450 °C, as seen in Fig. 1(D). The absence of diffraction ring patterns suggests all the grains in Cu film deposited at 450 °C have the same (1 0 0) orientation as the NaCl substrate. These observations indicate that the orientations of grains in the Cu films are dependent on the substrate temperature and Cu epitaxy is promoted at higher temperatures.

Additional diffraction spots or rings surrounding the Cu reflections can be also seen in the electron diffraction patterns shown in Fig. 1. These diffraction spots and rings are from native oxide (Cu_2O) layer formed on the Cu surfaces at room temperature in air during the TEM sample preparation. It is interesting to note from the electron diffraction patterns in Fig. 1 that the orientations of the native oxide layers follow the similar trend of the orientations of Cu grains in the Cu films deposited at the different temperatures. It can be seen that the Cu films with the relatively poor epitaxy result in Cu_2O diffraction rings of the oxide layer (*i.e.*, Fig. 1(A) and (B)), while the Cu films deposited at the higher temperatures (Fig. 1(C) and (D)) give the spot pattern of Cu_2O, indicating the enhanced epitaxy of the oxide layer.

This dependence of the film epitaxy on the substrate temperature during the deposition can be understood through the heterogeneous nucleation theory. Epitaxial Cu film deposition often follows 3-D island growth at elevated temperature [20–22]. For island growth mode, the concentration of adsorbed atoms is often very low, due to fast re-evaporation from the weakly binding substrate, and a large positive chemical potential change ($\Delta\mu$), or supersaturation, S, is needed to nucleate the deposit [23]. The nucleation barrier for a 3-D Cu embryo on the NaCl surface can be written as,

$$\Delta G^* = \frac{16\pi\sigma_{NG}^3}{3\Delta\mu^2} f(n) \qquad (1)$$

where σ_{NG} denotes the specific interfacial energy between nucleus and Cu vapor, and $f(n) = [(2+n)(1-n)^2/4]$ is the geometrical factor for a plane surface [24]. n depends on the interaction and structural match between the nucleus and the substrate. For a given system, the strong interaction and ideal structural match (*i.e.*, epitaxial nucleation) leads to $n \to 1$; on the other hand, the weak interaction and poor structural match (*i.e.*, nonepitaxial nucleation) leads to $n \to -1$ [25–28]. $\Delta\mu$ is related to the substrate temperature T_s by $\Delta\mu = kT_s \ln(p/p_e)$, and p/p_e is predominated by vacuum condition during the evaporation. In Fig. 2 the nucleation barrier ΔG^* is plotted via n for different T_s for the nucleation of a Cu island for a constant chemical potential change $\Delta\mu$. As can be seen from the plots, to minimize the nucleation barrier, epitaxial islands (*i.e.*, $n = 1$) is preferred for the high substrate temperature, *e.g.*, 450 °C. With decreasing substrate temperature, the nucleation barrier for nonepitaxial oxide islands ($n \to 0$, and -1) is lowered and the difference between the nucleation barriers of epitaxial and nonepitaxial Cu islands is significantly reduced. Therefore, both epitaxial and nonepitaxial Cu islands can be nucleated simultaneously on the substrate at lower temperature, *e.g.*, 150 °C. It is also noted from Fig. 2, even at the temperature as low as 150 °C, there is still considerate difference between the nucleation barriers of non-epitaxial and epitaxial oxide islands, suggesting that epitaxial Cu islands are still dominated in the film growth. This is consistent with our experimental observations as shown in Fig. 1(A) and (B), which show that the diffraction spots associated with epitaxial Cu grains have much stronger intensity than diffraction rings from randomly oriented Cu grains.

3.2. Cu surface morphology

The surface morphology of the Cu film depends on the deposition conditions such as temperature and evaporation rate. The NaCl substrates used are freshly cleaved from single crystal cubes, their measured surface roughness R_{RMS} is less than 1 nm. AFM is used to investigate the effect of deposition temperature on surface morphology of the Cu films. Fig. 3 shows the surface topography of Cu films formed on NaCl(1 0 0) substrates at different deposition temperatures. The surface roughness of the Cu films shows dramatic dependence on deposition temperature, *i.e.*, the surface flatness can be improved by lowering the substrate temperature. It can be also seen that the grain sizes of Cu film decreases with decreasing the deposition temperature.

Smooth and epitaxial metal films are usually desired for many other technological applications. However, the above results show that good epitaxy and smooth surface of Cu films cannot be achieved by the simple one-step deposition process. A three-step growth process developed by Wagner [29] is thus adopted to deposit Cu(1 0 0) films on NaCl(1 0 0) substrates. This method has been demonstrated effective for the Pt/Pd-$SrTiO_3$ film-substrate system [15]. The detailed process with a few modifications in our work is described as follows. We first grow Cu seeds at 450 °C that favors epitaxial Cu grains. Subsequently, the seeds are overgrown to form a continuous Cu film at the lower temperature ~150 °C that favors smooth Cu film. Once the desired film thickness (~700 Å) is reached, the film is then annealed for 1 h at 450 °C, resulting in epitaxial single-crystal Cu films: (1 0 0) NaCl||(1 0 0)Cu, [0 1 0]NaCl||[0 1 0]Cu. The quality of the Cu films by this three-step deposition process is examined by both AFM and TEM. Fig. 4(A) shows an AFM topographic image, which reveals that the as-deposited Cu film show small grains with a much reduced surface roughness of ~1.82 nm. An additional annealing of the as-deposited Cu film at 500 °C for 30 min results in even smoother film with a surface toughness of ~0.71 nm, as shown in Fig. 4(B). The bright-field TEM images and corresponding SAED patterns of as-deposited and annealed Cu film are also shown in Fig. 4(C) and (D), which confirm the film continuity and (0 0 1) film epitaxy. It is observed that after the annealing at 500 °C, the native oxide layer as well as defects, *e.g.*, stacking faults (the regions with bright–dark fringe contrast shown in Fig. 4(C)) in the Cu film is eliminated, resulting in a flat and clean Cu surface as shown in Fig. 4(D).

3.3. Effect of Cu surface conditions on the initial-stage oxidation of Cu

The initial oxidation of a metal surface involves various atomic and nanoscale surface processes including oxygen chemisorption, surface diffusion and oxide nucleation and growth. These processes are not solely governed by experimental variables, *i.e.*, oxygen pressure and oxidation temperature but also highly dependent on the metal surface conditions such as the surface orientations,

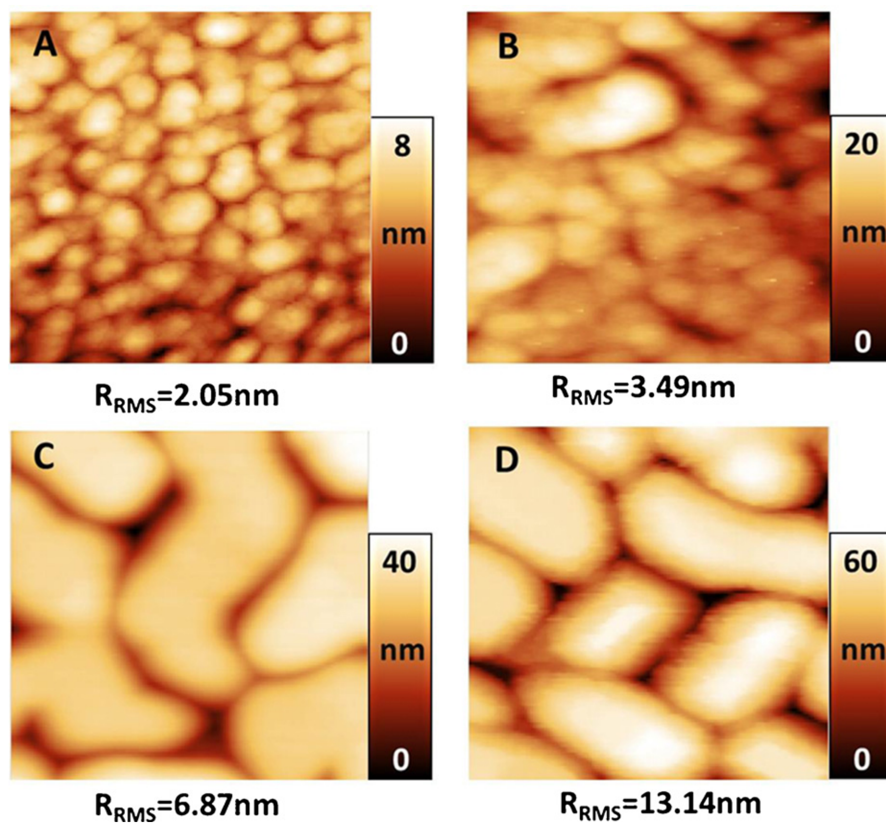

Fig. 3. AFM height images and surface roughness of Cu films deposited on NaCl(1 0 0) substrate at (A)150 °C, (B)250 °C, (C)350 °C, and (D)450 °C. Image size are all 500 nm × 500 nm.

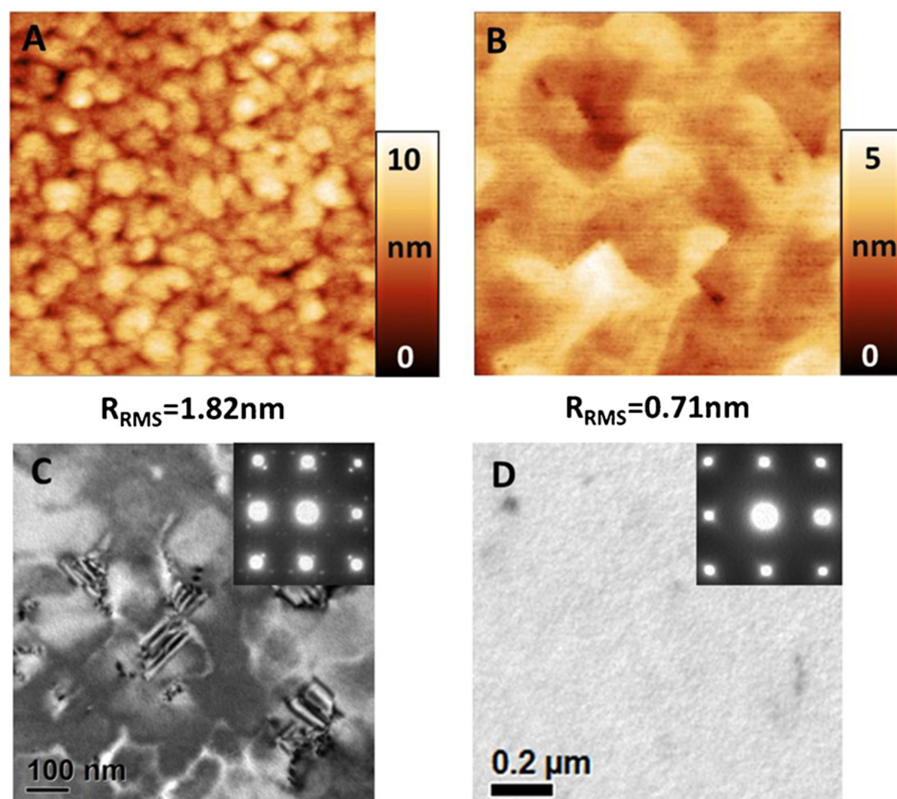

Fig. 4. AFM topographic images of (A) an as-deposited Cu film, (B) an Cu film annealed at 500 °C for 30 min using the three-step deposition process, image size are all 1 µm × 1 µm; Corresponding TEM images and SAED patterns of the as-deposited and annealed Cu films are shown in C and D, respectively.

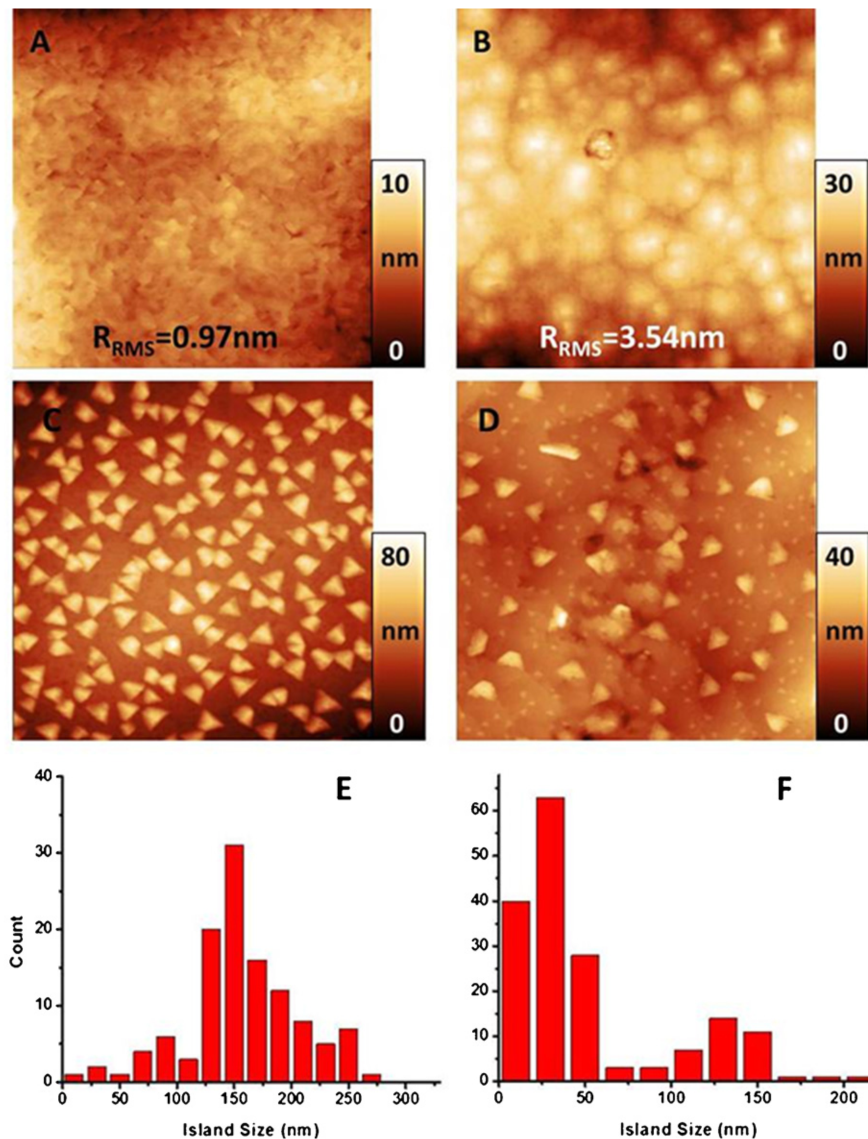

Fig. 5. Comparison of oxides formation on Cu surfaces prepared by the three-step process deposition (A, C and E) and the single-step process deposition (B, D and F). AFM topographic images of annealed Cu films (A and B); oxide islands formed after 30-min oxidation at 350 °C and $pO_2 = 5 \times 10^{-4}$ Torr (C and D) and the size distribution of the oxide islands (E and F), respectively. The lateral size of the images is 5 μm × 5 μm.

morphology, and roughness. Surface imperfections can strongly influence oxygen adsorption, surface diffusion and oxide nucleation. This is especially true if there is a high nucleation barrier for a perfect terrace. Then the barrier will often be by-passed on a real surface by special sites such as step-edges [23,30–32].

In order to elucidate the effect of the surface conditions on the early stages of Cu oxidation, two different Cu(1 0 0) surfaces are prepared using the single-step process and three-step process as described above. The Cu films are first checked by AFM right after the deposition, and then loaded into the TEM chamber for *in situ* annealing at 500 °C for 30 min, and re-examined by AFM after the annealing. For the Cu films grown by the one-step deposition process, the R_{RMS} surface roughness of the film decreases from ∼6.87 nm to ∼3.54 nm after annealing at 500 °C; for the Cu films grown by the three-step deposition process, the R_{RMS} surface roughness changes from ∼1.82 nm to ∼0.71 nm after annealing at 500 °C. Fig. 5(A) and (B) shows representative AFM topographic images of the surfaces of the two types of Cu films generated by the three-step and single-step deposition processes. The morphology of the annealed Cu films shows flat surface with small surface steps for the three-step process (Fig. 5(A)) while rough surface with relatively large grains for single-step process (Fig. 5(B)).

The above Cu(1 0 0) films are then oxidized at 350 °C in $pO_2 = 5 \times 10^{-4}$ Torr for 30 min. Oxide island formation occurs for both Cu surfaces, as shown by the AFM images in Fig. 5(C) and (D). Fig. 5(E) and (F) shows the size distribution of oxide islands measured from the AFM images (note that the size of oxide islands is measured as the disk radius). It can be seen that oxide islands formed on the Cu film grown by the three-step deposition process have a triangular shape with an average size of ∼150 nm and a height of ∼30 nm. However, oxide islands formed on the Cu film grown by the single-step deposition exhibit a triangular shape but have a bi-modal distribution of the island size: large islands (∼25% of the total oxide islands) have an average size of ∼130 nm and a height of ∼10 nm while small islands have a lateral size of ∼25 nm and a height of just 5–8 nm.

The growth features of the Cu films and the subsequent oxidation of the Cu films are also examined by *in situ* TEM. As shown

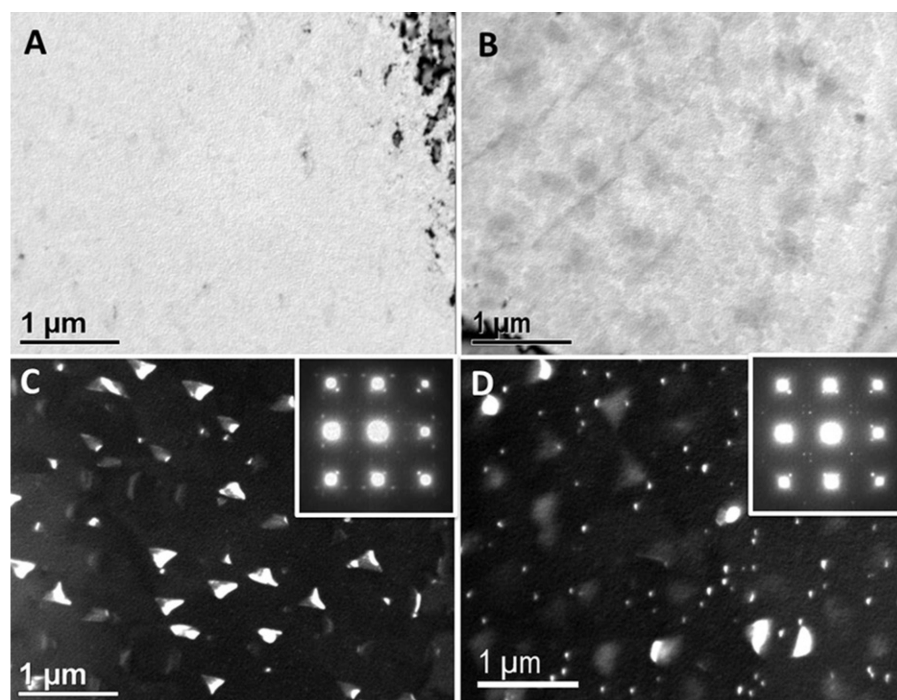

Fig. 6. Bright-field TEM images of annealed Cu films prepared by (A) three-step process deposition; (B) single-step process deposition; dark-field TEM images (using $Cu_2O(2\,2\,0)$ reflection) of oxide islands from the oxidation of the annealed Cu film by three-step process deposition (C); and oxide islands from the oxidation of the annealed Cu film by single-step process deposition (D). Inserts are SAED patterns of the oxidized Cu films.

in Fig. 6, Cu films prepared by the three-step deposition process show relatively uniform TEM contrast due to the homogeneous film structure, while the Cu film grown by the single-step deposition show fine bright/dark fringe TEM contrast due to presence of film imperfections (*e.g.*, grain boundaries or non-uniform film thickness). The corresponding dark-field TEM images of the oxidized Cu films show relatively uniform size distribution of oxide islands formed on the Cu film grown by the three-step deposition process while a bi-modal distribution of the sizes of oxide islands on the oxidized Cu film grown by the single-step deposition. These features are consistent with the AFM observations as shown in Fig. 5. However, the SAED patterns indicate that the Cu_2O oxide islands formed on both surfaces have a cube-on-cube orientation relation with the Cu(0 0 1) substrate.

This non-uniform size distribution of triangle Cu_2O islands on the Cu films prepared by the single-step deposition process suggests the oxide growth can be inhibited at specific sites during the oxidation. It is reasonable to expect a larger nucleation density on rough surfaces because the nucleation events are preferred at low-coordinated surface sites such as steps and kinks with a lower nucleation barrier. Once stable oxide islands are formed, the oxide growth relies on oxygen surface diffusion to the edge of oxide nuclei for incorporating into the oxide by reacting with adjacent Cu atoms. The lack of efficient oxygen surface diffusion slows down the oxide growth for oxide islands nucleated on the rough surface regions. Yang et al. [33–35] proposed an oxygen surface diffusion model to describe oxide island growth during the initial stages of Cu oxidation. After some incubation time, the nucleation of oxide islands begins and the density of stable oxide nuclei increases with the time, reaching a saturation density, $N_s = 1/L_d^2$, where L_d^2 is the area of the "zone of oxygen capture" around each Cu_2O island. An oxygen concentration gradient exists across this zone such that oxygen that lands within this zone shall diffuse to the Cu_2O islands; hence, the oxide islands act as oxygen sinks. The probability of an oxide nucleation event is proportional to the fraction of the available surface area outside these "zones of oxygen capture" and the oxide nucleus density can be determined to be [36]

$$N = \frac{1}{L_d^2}(1 - e^{-kL_d^2 t}) \tag{2}$$

where k is the initial nucleation rate, which depends on the probability for Cu and O to form Cu_2O at the oxidation temperature, and t is the oxidation time. Due to the enhanced mobility of surface atoms at a higher temperature, it is reasonable to expect an Arrhenius dependence of the nucleation density of oxide nuclei on the oxidation temperature as [35]

$$N \sim e^{-E_a/kT} \tag{3}$$

where k is Boltzmann's constant, T is the oxidation temperature, and E_a is the activation energy for oxide nucleation. By measuring the island density at different oxidation temperatures, the activation energy, E_a, can be determined. Note that the nucleation activation energy depends on the energies of nucleation, adsorption and/or desorption of oxygen, and not necessarily only on the oxygen surface diffusion energy.

In situ TEM observation of the early stages of oxidation of Cu films under different oxidation temperatures are made to obtain the saturated density of oxide islands and the growth kinetics of oxide islands. Fig. 7 presents a sequence of *in situ* dark-field TEM images captured from an *in situ* video of Cu oxidation that clearly shows the growth of oxide islands on Cu(1 0 0) film prepared by the single step process. Both morphological evolution and growth rate of oxide islands can be obtained from the video. Using these *in situ* TEM observations, the number density of oxide islands can be determined as a function of the oxidation conditions. Fig. 8 shows the Arrhenius dependence of nucleation density on temperature plotted for the oxidation at $pO_2 = 5 \times 10^{-4}$ Torr and the temperature ranging from 250 °C to 450 °C for the Cu(1 0 0) films prepared by the single-step and three-step deposition processes. E_a for the oxide nucleation on these two surfaces is determined

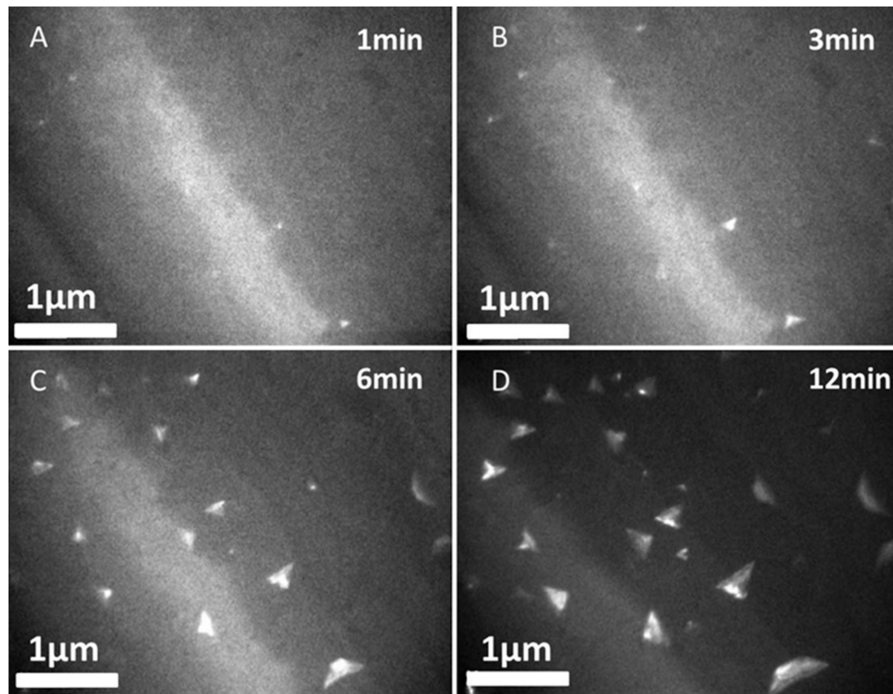

Fig. 7. *In situ* dark field TEM images (using $Cu_2O(2\,2\,0)$ reflection) of Cu oxide islands formed on the Cu(1 0 0) thin film prepared by single-step process deposition, where the oxidation condition is $T = 350\,^{\circ}C$ and $pO_2 = 5 \times 10^{-4}$ Torr.

to be 1.4 ± 0.1 eV and 1.2 ± 0.15 eV, respectively, by the slope of the plots in Fig. 8. The obtained activation energies determined above are the average value for the oxide islands on the entire surface. These results indicate the nucleation activation energy depends on the surface morphology, *i.e.*, the flat surface prepared by the three-step deposition process requires a larger oxide nucleation barrier. The rough Cu surface prepared by the single-step deposition process provides large amount of surface imperfections, which results in a lower nucleation barrier.

The *in situ* TEM video showing the size evolution of oxide islands as a function of oxidation time can be also quantified to examine the effect of surface morphology on the oxide growth. The temporal evolution of the cross-sectional area of oxide islands is plotted for the oxidation of Cu thin films prepared by the single-step and three-step deposition processes, as shown in Fig. 9. Note that the oxidation of Cu film prepared by the single-step deposition results in bi-modal size distribution of oxide islands (*i.e.*, large and small islands, seen in Fig. 5) and their size evolution is thus measured separately. The growth rates of the three types of oxide islands are shown in Fig. 9, which clearly reveal slower growth rates for the oxide islands formed on the rough Cu surface. While the oxide islands formed on these surfaces show a nearly linear growth behavior that, suggests 3D island growth controlled by oxygen surface diffusion [33], and the faster growth rate of the oxide islands on the flat Cu surface prepared by the three-step process deposition suggests more efficient oxygen surface diffusion controlling the oxide island growth.

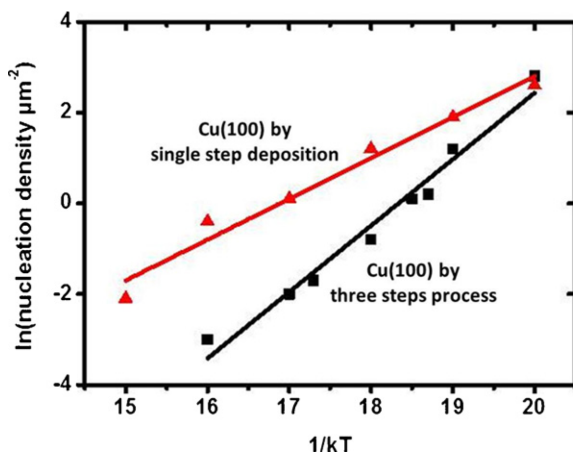

Fig. 8. Arrhenius plots of the saturation density of oxide islands from the oxidation of the Cu films prepared by single-step process deposition (triangular symbol) and three-step process deposition (square symbol). The oxidation condition is $pO_2 = 5 \times 10^{-4}$ Torr and $T = 250–450\,^{\circ}C$ for 30 min.

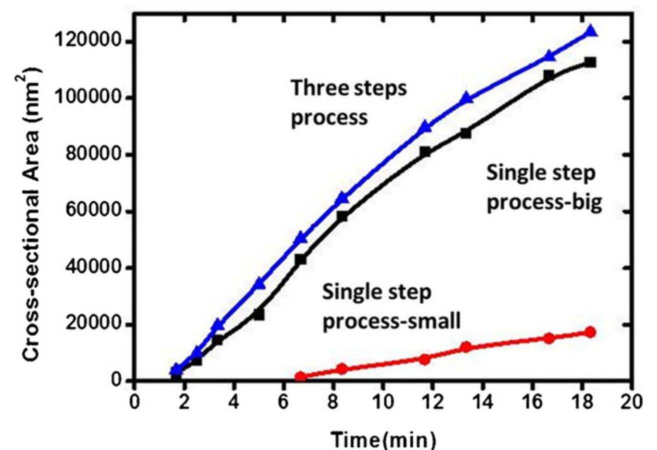

Fig. 9. Cross-sectional areas of oxide islands *vs.* oxidation time for the oxidation of Cu(1 0 0) thin films prepared by single-step process deposition (square symbol for big islands, round symbol for small islands) and three-step process deposition (triangle).

4. Conclusion

We have shown that the epitaxial growth of Cu films on NaCl substrates can be significantly influenced by deposition temperature, *i.e.*, higher temperature results in good film epitaxy but larger roughness and *vice versa*. The surface roughness of Cu films can be dramatically decreased by three step process deposition without sacrificing the film epitaxy. The effect of the resulting Cu films by the different growth conditions on the early stages oxidation of Cu is examined by *in situ* TEM and *ex situ* AFM. It is found that surface condition can have dramatic influence on the early stages oxidation behaviors of Cu films that not only results in different growth morphologies of oxide islands but also distinct variations in the oxide nucleation density and growth rates. This effect of surface condition gives insights into understanding the mechanism of the transient oxidation of metals and manipulating the initial oxide formation through surface treatment for potential technological applications.

Acknowledgements

Research was supported by the U.S. Department of Energy, Office of Basic Energy Sciences, Division of Materials Sciences and Engineering under Award No. DE-FG02-09ER46600.

References

[1] M.W. Bench, P.G. Kotula, C.B. Carter, Surface Science 391 (1997) 183.
[2] H. Huang, H.L. Wei, C.H. Woo, X.X. Zhang, Applied Physics Letters 82 (2003) 4265.
[3] Y.P. Zhao, G.C. Wang, T.M. Lu, G. Palasantzas, J.T.M. De Hosson, Physical Review B 60 (1999) 9157.
[4] J.-N. Sun, Y. Hu, W.E. Frieze, W. Chen, D.W. Gidley, Journal of the Electrochemical Society 150 (2003) F97.
[5] C. Jonda, A.B.R. Mayer, U. Stolz, A. Elschner, A. Karbach, Journal of Materials Science 35 (2000) 5645.
[6] J. Chao, J.L. González-Carrasco, Materials Science and Engineering: A 230 (1997) 39.
[7] D.C. Lim, Y.D. Kim, Applied Surface Science 253 (2006) 2984.
[8] J. Li, J.W. Mayer, E.G. Colgan, Journal of Applied Physics 70 (1991) 2820.
[9] W.A. Lanford, P.J. Ding, W. Wang, S. Hymes, S.P. Murarka, Materials Chemistry and Physics 1995 (1995) 192.
[10] S.K. Lahiri, N.K. Waalib Singh, K.W. Heng, L. Ang, L.C. Goh, Microelectronics Journal 29 (1998) 335.
[11] D. Tracy, D. Knorr, Journal of Electronic Materials 22 (1993) 611.
[12] D.P. Tracy, D.B. Knorr, K.P. Rodbell, Journal of Applied Physics 76 (1994) 2671.
[13] K.-W. Kwon, C. Ryu, R. Sinclair, S.S. Wong, Applied Physics Letters 71 (1997) 3069.
[14] H.L. Wei, H. Huang, C.H. Woo, R.K. Zheng, G.H. Wen, X.X. Zhang, Applied Physics Letters 80 (2002) 2290.
[15] A.J. Francis, Y. Cao, P.A. Salvador, Thin Solid Films 496 (2006) 317.
[16] G. Zhou, PhD Thesis, Department of Materials Science and Engineering, University of Pittsburgh, Pittsburgh, 2003.
[17] G. Zhou, J.C. Yang, Surface Science 559 (2004) 100.
[18] G.W. Zhou, J.C. Yang, Physical Review Letters 93 (2004) 226101.
[19] G.W. Zhou, W.Y. Dai, J.C. Yang, Physical Review B 77 (2008) 245427.
[20] M.J. Gibson, P.J. Dobson, Journal of Physics F: Metal Physics 5 (1975) 864.
[21] M. Böhringer, Q. Jiang, R. Berndt, W.D. Schneider, J. Zegenhagen, Surface Science 367 (1996) 245.
[22] B. Müller, L. Nedelmann, B. Fischer, H. Brune, J.V. Barth, K. Kern, Physical Review Letters 80 (1998) 2642.
[23] J.A. Venables, G.D.T. Spiller, M. Hanbucken, Reports on Progress in Physics 47 (1984) 399.
[24] I.V. Markov, Crystal Growth for Beginners: Fundamentals of Nucleation, Crystal Growth and Epitaxy, 2nd edition, World Scientific, River Edge, NJ, USA, 2003.
[25] D. Turnbull, B. Vonnegut, Industrial and Engineering Chemistry 44 (1952) 1292.
[26] X.Y. Liu, Journal of Chemical Physics 111 (1999) 1628.
[27] X.Y. Liu, Journal of Chemical Physics 112 (2000) 9949.
[28] X.Y. Liu, Langmuir 16 (2000) 7337.
[29] T. Wagner, G. Richter, M. Ruhle, Journal of Applied Physics 89 (2001) 2606.
[30] C.H. Chung, H.W. Yeom, B.D. Yu, I.W. Lyo, Physical Review Letters 97 (2006) 036103.
[31] J. Klikovits, M. Schmid, L.R. Merte, P. Varga, R. Westerström, A. Resta, J.N. Andersen, J. Gustafson, A. Mikkelsen, E. Lundgren, F. Mittendorfer, G. Kresse, Physical Review Letters 101 (2008) 266104.
[32] J.T. Yates, Journal of Vacuum Science & Technology A: Vacuum, Surfaces, and Films 13 (1995) 1359.
[33] J.C. Yang, M. Yeadon, B. Kolasa, J.M. Gibson, Applied Physics Letters 70 (1997) 3522.
[34] J.C. Yang, B. Kolasa, J.M. Gibson, Applied Physics Letters 73 (1998) 2841.
[35] J.C. Yang, M.D. Bharadwaj, G. Zhou, L. Tropia, Microscopy & Microanalysis 7 (2001) 486.
[36] J.C. Yang, M. Yeadon, B. Kolasa, J.M. Gibson, Scripta Materialia 38 (1998) 1237.